# Parameterization of unresolved obstacles in wave modelling: a source term approach

Mentaschi L.[a,c,*], Pérez J.[b], Besio G.[a], Mendez F. J.[b], Menendez M.[b]

[a] *DICCA, Dipartimento di Ingegneria Civile, Chimica e Ambientale, Università degli Studi di Genova, via Montallegro 1, 16145 Genova, Italy*
[b] *Environmental Hydraulics Institute (IH Cantabria), Universidad de Cantabria, c\Isabel Torres 15, 39011, Santander, Spain.*
[c] *INFN, Istituto Nazionale di Fisica Nuclare, Sezione di Genova, Via Dodecaneso 33, 16146, Genova, Italy*

**Abstract**

In the present work we introduce two source terms for the parameterization of energy dissipation due to unresolved obstacles in spectral wave models. The proposed approach differs from the classical one based on spatial propagation schemes because it provides a local representation of phenomena such as unresolved wave energy dissipation. This source term-based approach presents the advantage of decoupling unresolved obstacles parameterization from the spatial propagation scheme, allowing not to reformulate, reimplement and revalidate the parameterization of unresolved obstacles for each propagation scheme. Furthermore it opens the way to parameterizations of other unresolved sheltering effects like rotation and redistribution of wave energy over frequencies. Proposed source terms estimate respectively local energy dissipation and shadow effect due to unresolved obstacles. Source terms validation through synthetic case studies has been carried out, showing their ability in reproducing wave dynamics comparable to those of high resolution models. The analysis of high resolution stationary wave simulations may help to better diagnose and study the effects of unresolved obstacles, providing estimations of transparency coefficients for each spectral component and allowing to understand and model unresolved effects of rotation and redistribution of wave energy over frequencies.

*Keywords:* Wave modelling, WAVEWATCH III®, Unresolved obstacles, Energy dissipation, Wave sheltering

## 1. Introduction

Unresolved obstacles (small islands, cliffs, shoals ...) are a main source of local error in spectral wave modelling (Tolman, 2001, 2002, 2014). In presence of a coast with complex bathymetry local errors can accumulate and affect vast portions of the domain (e.g. Hardy and Young, 1996; Ponce de León and C., 2005; Tuomi et al., 2014; Mentaschi et al., 2015). An established approach to solve this issue has been proposed by Booij et al. (1999) and implemented in SWAN® model (Holthuijsen et al., 2001) and in WAVEWATCH III® model (hereinafter referred to as WWIII, Tolman, 2014, 2003; Chawla and Tolman, 2008). This approach consists in correcting energy fluxes estimated by the spatial propagation scheme on the basis of transparency coefficients of obstructed cells. A similar approach has been implemented by Hardy et al. (2000) in WAM model, introducing transparency coefficients modulated as functions of spectral component direction, though Chawla and Tolman (2008) showed that transparency coefficients defined per main grid axis are accurate enough in most cases.

This approach improves significantly wave model performances, but at the same time its use leads to some drawbacks. Sheltering due to unresolved obstacles is mainly a local effect, hence a local parameterization by a source term may be a good alternative to a description in the propagation scheme. In the approach described by Tolman (2003) a cell transparency coefficient $\alpha$ is applied partly to reduce the ingoing energy flux at the upstream border, partly to reduce the outgoing flux at the downstream border, using a rule completely independent from the layout of the unresolved obstacles inside the cell. As a result the estimated net energy flux throughout the cell is correct; however, the

*Corresponding author. Address: DICCA, Via Montallegro 1, 16145, Genova, Italy
*Email address:* lorenzo.mentaschi@unige.it (Mentaschi L.)

resulting average energy is not always rigorously represented. Imposing different values for upstream and downstream transparencies may help to overcome this issue, but the physical meaning of upstream and downstream transparency is not always straightforward. Drawbacks of representing local effects in the propagation scheme are also possible in regular grids where the flux is decomposed and propagated separately to $y$ and $x$ directions. An example is illustrated in figure 1. Here energy travels from the bottom-left cell to the top-right cell, and should not encounter any obstacle on its path. However, as a result of flux decomposition in y and x directions, system behaves as if top-left obstruction (the brown dot in the figure) was on energy path.

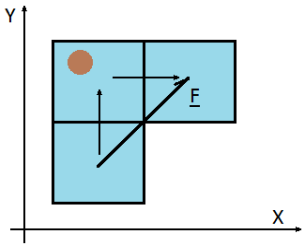


Figure 1: Propagation scheme drawback: the energy flux for an oblique spectral component is reduced by an obstacle (the brown spot) that is not on the real path of the energy

Another drawback of using approaches based on the propagation scheme is that the sheltering effects of unresolved features involve not only energy dissipation, but also rotation of spectral components and redistribution of energy over frequencies due to unresolved refraction/diffraction. Since propagation scheme propagates separately each spectral component it would be difficult to model through it transformations of the whole spectrum such as rotations. Conversely in an approach based on a source term the whole propagated spectrum is available, allowing parameterization of rotations and redistribution of wave energy over frequencies as a future development.

The introduction of propagation schemes allowing unstructured grids with varying resolution like finite elements propagation scheme (Roland, 2008), or spherical multiple-cell propagation scheme (Li, 2012), partially overcomes the problem of unresolved obstacles, but it is not always computationally convenient to increase resolution in proximity of all the obstacles existing in the domain.

In this study we introduce a new source term approach to parameterize the energy dissipation due to unresolved obstacles on the basis of transparency coefficients estimated for each obstructed cell/spectral component. The first source term models the average local dissipation (LD), while a second source term models the shadow effect (SE) of an obstructed cell towards the downstream cells.

The present manuscript is organized as follows: the LD-SE scheme is formulated in sections 2.1, 2.2 and 2.3 and the performances of the source terms couple are assessed in section 3 on the basis of simple theoretical cases. Discussion of the obtained results is presented in section 4 and some final conclusions are drawn in section 5.

## 2. The Local Dissipation and Shadow Effect scheme (LD-SE)

As mentioned above unresolved obstacles can involve different effects, ranging from energy dissipation to spectral components rotation and redistribution of wave energy over frequencies due to unresolved refraction-diffraction effects. In the following sub-sections the description of the source terms formulation for local dissipation and shadow effect due to unresolved obstacles will be presented.

### *2.1. The Local Dissipation (LD) source term*

Following previous works about the parameterization of unresolved obstacles (e.g. the already cited Booij et al., 1999; Hardy et al., 2000; Holthuijsen et al., 2001; Tolman, 2003; Chawla and Tolman, 2008), this formulation relies on the concept of transparency coefficient $\alpha$ of an obstructed cell. Let us consider a cell and a spectral component directed in the $x$ direction, as represented in figure 2. In stationary conditions and under the hypotheses of null wind wave growth and null resolved dissipation the coefficient of transparency $\alpha$ of the cell is defined as the ratio between

the spectral energy density exiting the cell ($F_d$, where the suffix $d$ stands for downstream) and the spectral energy density entering the cell ($F_u$, where the suffix stands for upstream):

$$\alpha = F_d / F_u \ . \tag{1}$$

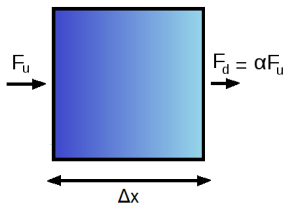


Figure 2: $1 - \alpha$ source term

The energy loss rate of the cell is proportional to the attenuation coefficient $(1 - \alpha)$ and to the distance covered by the mode in a time unit. Hence the dissipation rate by unit length is given by:

$$\left.\frac{\partial F}{\partial t}\right|_{\alpha} = -(1-\alpha)\frac{c_g}{\Delta x} F_u \ , \tag{2}$$

where $\Delta x$ is the $x$ span of the cell. Since a spectral wave model does not estimate the upstream energy density $F_u$, expression (2) must be expressed in terms of the average energy $F$ of the cell. If the dissipation is constant across the cell, the average spectral density $F$ of the cell is given by the average between $F_u$ and $F_d$:

$$F = \frac{F_u + F_d}{2} = \frac{1+\alpha}{2} F_u \ . \tag{3}$$

Using expression (3) to eliminate $F_u$ from (2) we obtain the $1 - \alpha$ source term:

$$\left.\frac{\partial F}{\partial t}\right|_{\alpha} = -2\frac{1-\alpha}{1+\alpha}\frac{c_g}{\Delta x} F \ . \tag{4}$$

Source term given by expression (4) describes local dissipation using the sole overall transparency coefficient of the cell. However using a single $\alpha$ coefficient for each spectral component is not enough to estimate accurately the average energy loss of the cell. Let us consider for example a situation where all the unresolved obstacles are concentrated in the downstream half of the cell, and the first half of the cell is not involved in the energy dissipation. The use of the $1 - \alpha$ source term, which models an energy dissipation continuously distributed throughout the cell, leads to an underestimation of the cell average energy. An analogous argument for the opposite situation of unresolved obstacles concentrated in the upstream half of the cell leads to the conclusion that in this case the $1 - \alpha$ source term tends to overestimate the average energy.

A more accurate estimate of the cell average energy may be achieved subdividing the cell in two halves and considering a transparency coefficient for each half. Figure 3 illustrates the new configuration. We consider a spectral component directed in the $x$ direction. The transparency coefficients $\alpha_1$ and $\alpha_2$ are associated to the two halves of the cell respectively. $F_{u1}$, $F_{d1}$ and $F_1$ represent the upstream, downstream and average spectral densities of the first half of the cell while $F_{u2}$, $F_{d2}$ and $F_2$ have the same meaning for the second half. The contribution of each half cell can be computed separately using similar arguments to those outlined previously:

$$\left.\frac{\partial F}{\partial t}\right|_{\alpha_1} = -2\frac{1-\alpha_1}{1+\alpha_1}\frac{c_g}{\Delta x} F_1 \quad , \tag{5}$$

$$\left.\frac{\partial F}{\partial t}\right|_{\alpha_2} = -2\frac{1-\alpha_2}{1+\alpha_2}\frac{c_g}{\Delta x} F_2 \quad . \tag{6}$$

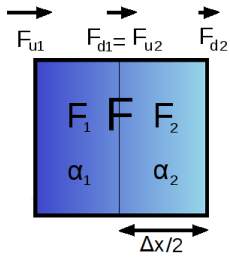


Figure 3: $2-\alpha$ source term

Since dissipation in the upstream half of the cell affects the whole cell, while dissipation in the downstream half of the cell affects only half cell, it is reasonable to average the two contributions in a whole-cell source term as:

$$\left.\frac{\partial F}{\partial t}\right|_{\alpha_1\alpha_2} = \left(\phi_1 \left.\frac{\partial F}{\partial t}\right|_{\alpha_1} + \phi_2 \left.\frac{\partial F}{\partial t}\right|_{\alpha_2}\right) \tag{7}$$

where $\phi_1 = 1$ and $\phi_2 = 1/2$.

Since

$$F_1 = \frac{F_{u1} + F_{d1}}{2} \quad , \quad F_2 = \frac{F_{u2} + F_{d2}}{2} \tag{8}$$

and

$$F_{d1} = \alpha_1 F_{u1} \ , \ \ F_{u2} = F_{d1} \ , \ \ F_{d2} = \alpha_2 F_{u2} = \alpha_1\alpha_2 F_{u1} \tag{9}$$

where $F_i$ is the average energy of the $i^{th}$ half, and $F_{ui}$ and $F_{di}$ are the incoming and outgoing energy density at the borders of the $i^{th}$ half, and since

$$F = \frac{F_1 + F_2}{2} \ , \tag{10}$$

we can express $F_1$ and $F_2$ as functions of $F$ and obtain from relationships (5), (6) and (7) an expression for the $2-\alpha$ source term:

$$\left.\frac{\partial F}{\partial t}\right|_{\alpha_1\alpha_2} = -4\frac{1 - \frac{\alpha_1+\alpha_1\alpha_2}{2}}{1 + 2\alpha_1 + \alpha_1\alpha_2}\frac{c_g}{\Delta x}F \quad . \tag{11}$$

It is straightforward to verify that the source term given by relationship (11) in the limit case of $(\alpha_1 = 1, \alpha_2 < 1)$, which represents a configuration where all the obstructions lie in the second half of the cell, models a smaller average energy loss than estimated by source term of expression (4). Conversely in the opposite case of $(\alpha_1 < 1, \alpha_2 = 1)$, which represents a configuration where all the obstructions lie in the first half of the cell, the $2-\alpha$ source term models a greater local effect than the $1-\alpha$ source term.

The arguments outlined in expressions (5)-(11) can be extended to estimate a $N$-$\alpha$ source term, i.e. obtained subdividing of the cell in $N$ slices, each with its transparency $\alpha_i$. In such a case the weighting factors $\phi_i$ are given by

$$\phi_i = \frac{N - i + 1}{N} \tag{12}$$

and the contribution of all the slices are averaged to compute a whole-cell source term as

$$\left.\frac{\partial F}{\partial t}\right|_{N} = \sum_{i=1}^{N} \phi_i \left.\frac{\partial F}{\partial t}\right|_{i} \ . \tag{13}$$

Result is (see Appendix A for details)

$$\left.\frac{\partial F}{\partial t}\right|_{N} = -2N\frac{1 - \frac{\sum_{i=1}^{N}\prod_{i=1}^{N}\alpha_i}{N}}{1 + 2\left(\sum_{i=1}^{N-1}\prod_{j=1}^{i}\alpha_j\right) + \prod_{i=1}^{N}\alpha_i}\frac{c_g}{\Delta x}F \quad . \tag{14}$$

Expression (14) gets more readable and understandable if we consider that quantity $\prod_{j=1}^{i} \alpha_j$ represents the transparency $A_i$ of the cell portion up to the $i^{th}$ section:

$$A_i = \prod_{j=1}^{i} \alpha_j \ . \tag{15}$$

If we define the coefficient $\beta$ as the average value of $A_i$ across the cell, $\beta = \sum A_i / N$ we obtain expression:

$$\left.\frac{\partial F}{\partial t}\right|_N = -2\frac{N(1-\beta)}{1+2N\beta-\alpha}\frac{c_g}{\Delta x}F \tag{16}$$

where $\alpha$ represents the total transparency of the cell,

$$\alpha = \prod_{i=1}^{N} \alpha_i \ . \tag{17}$$

Expression (16) is equivalent to relationship (4) for $N = 1$ and to relationship (11) for $N = 2$.

If we estimate the limit value of (16) for $N \to \infty$, we are ready to state the generalized expression:

$$\left.\frac{\partial F}{\partial t}\right|_\infty = -\frac{1-\beta}{\beta}\frac{c_g}{\Delta x}F \ . \tag{18}$$

It is worth noting that in the "infinite $N$" case the source term depends from the sole $\beta$ parameter, which represents the average transparency of cell sections starting from the cell upstream side. A straightforward two dimension generalization of (18) is given by

$$\frac{\partial F}{\partial t} = -\frac{1-\beta}{\beta}\sqrt{\left(\frac{c_{gx}}{\Delta x}\right)^2 + \left(\frac{c_{gy}}{\Delta y}\right)^2}F \ . \tag{19}$$

It is necessary to remark that coefficients $\alpha$ and $\beta$ in general are not unique for a given cell, but may be function of the spectral component.

### 2.2. *The Shadow Effect (SE) source term*

The source term described above provides a representation of the current cell average energy balance, despite the fact that the effects of unresolved obstacles on the flux towards the downstream cell are neglected. Without further adjustments the spatial propagation scheme will propagate the average energy of the upstream cell, which in some cases can be very different from the energy really entering the downstream cell.

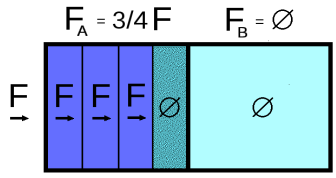


Figure 4: Shadow effect: the energy is totally blocked between the upstream cell and the downstream cell, and no energy enters the downstream cell.

As an example let us consider the situation illustrated in figure 4. In steady conditions the first three sections of the upstream cell A have a constant energy $F$, which is totally blocked in the last section by some obstruction. If the average energy of the last section is null, the average energy of cell A is $F_A = 3/4F$. In this situation the propagation scheme would propagate to the downstream cell B the average energy of A. A correct representation of the physical process would require instead a null transport of energy from cell A to cell B.

Therefore we introduce a source term in the downstream cell to adjust a posteriori the amount of energy transported from the upstream cell. This source term must be applied immediately after the space propagation, before the spectral

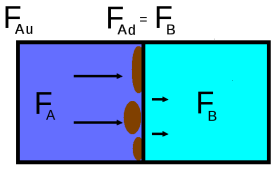


Figure 5: Shadow effect: obstacles at the border between cell A and cell B project their shadow towards cell B.

propagation scheme and all the other source terms, in order to provide the system for a correct amount of advected energy.

In the monodimensional situation illustrated in figure 5 the energy $E_{ps}$ advected from cell A to cell B by the propagation scheme during time step $\Delta t$ is

$$E_p = F_A \Delta y \, c_g \Delta t \, , \tag{20}$$

where $F_A$ is the average energy density of the cell A and the $p$ suffix stands for "propagated". But the energy really advected should be

$$E_d = F_{Ad} \Delta y \, c_g \Delta t \, , \tag{21}$$

where $F_{Ad}$ is the downstream energy density of the cell A and the suffix $d$ stands for "downstream". Hence adjustment to the total amount of energy of the downstream cell B in the time $\Delta t$ is:

$$\Delta E_B = -(F_A - F_{Ad}) \Delta y \, c_g \Delta t \, . \tag{22}$$

From expression (22) we can write an adjustment source term for the downstream cell:

$$\left. \frac{\partial F}{\partial t} \right|_B = -\frac{c_g}{\Delta x} (F_A - F_{Ad}) \quad . \tag{23}$$

In order to make the source term usable in a spectral wave model, we must express it as a function of the energy density $F_B$ of the cell B. We can accomplish this considering that in stationary conditions, if we neglect the active generation, wave dissipation and dispersion, and the effects of unresolved obstacles in the cell B, the relationship $F_{Ad} = F_B$ holds. In this case we can express $F_A$ as a function of $F_B$ using the $n - \alpha$ parameterization of the internal structure of the cell A, which is represented by coefficients $\alpha_A$ and $\beta_A$:

$$F_A = F_A(F_B, \alpha_A, \beta_A) \quad . \tag{24}$$

Hence expression (23) can be rewritten:

$$\left. \frac{\partial F}{\partial t} \right|_{d\,B} = -\frac{c_g}{\Delta x} [F_A(F_B, \alpha_A, \beta_A) - F_B] \quad , \tag{25}$$

where the suffix $d$ stands for "downstream". In (25) we neglected the active generation of wind sea in the cell B. If this hypothesis is not valid the average energy density of B is a sum of contributions of advection and local generation, and a direct application of relationship (25) would lead to an overestimation of dissipation. A possible solution may be a reduction of the shadow term by a factor $\psi$, which is a function of the wave age $v$ of the spectral component. If the wave age is high the spectral component is swell and the effect of the source term must be full:

$$\lim_{v \to \infty} \psi(v) = 1 \, . \tag{26}$$

In the case of a low wave age (e.g. $v < v_0 = 5$) the spectral component is wind generated and the effect of the source term should be reduced.

$$\psi(v < v_0) \ll 1 \quad . \tag{27}$$

Hence the monodimensional source term can be expressed as

$$\left. \frac{\partial F}{\partial t} \right|_d = -\psi(v) \, \frac{c_g}{\Delta x} \, [F_A(F_B, \alpha_A, \beta_A) - F_B] \quad . \tag{28}$$

### 2.2.1. $1-\alpha$ source term

Using relationships (1) and (3) we obtain:

$$F_A = \frac{1+\alpha}{2\alpha} F_{Ad} = \frac{1+\alpha}{2\alpha} F_B \quad . \tag{29}$$

Substituting this expression in relationship (28) we find the monodimensional source term:

$$\left.\frac{\partial F}{\partial t}\right|_{d\ \alpha_u} = -\psi(v)\ \frac{1-\alpha_u}{2\alpha_u}\frac{c_g}{\Delta x} F \quad , \tag{30}$$

where the suffix $u$ stresses the fact that $\alpha$ coefficient is relative to the upstream cell, and not to the current cell.

### 2.2.2. $N-\alpha$ source term

Using considerations similar to those outlined for relationships (5)-(11) and explained in more detail in Appendix A we can express $F_A$ as a function of $F_B$ in the case of $N-\alpha$, obtaining

$$F_A = \frac{1 + 2\left(\sum_{j=1}^{N-1}\prod_{l=1}^{j}\alpha_l\right) + \prod_{j=1}^{N}\alpha_j}{2N\prod_{j=1}^{N}\alpha_j} F_B \quad . \tag{31}$$

Substituting (31) in (28) we find an expression for the downstream source term in the $N-\alpha$ case:

$$\left.\frac{\partial F}{\partial t}\right|_{d} = -\psi(v)\left[\frac{1+2N(\beta_u-\alpha_u)-\alpha_u}{2N\alpha_u}\right]\frac{c_g}{\Delta x} F \ . \tag{32}$$

In the limit for $N\to\infty$ we obtain:

$$\left.\frac{\partial F}{\partial t}\right|_{d} = -\psi(v)\ \frac{c_g}{\Delta x}\left(\frac{\beta_u}{\alpha_u} - 1\right) F \quad . \tag{33}$$

It is worth noting that like the upstream source term described by relationship (18), the shadow infinite N source term depends only on coefficients $\alpha_u$ and $\beta_u$. Coefficient $\alpha_u$ represents the total transparency of the upstream cell and coefficient $\beta_u$ represents the average transparency of upstream cell sections starting from the cell upstream side.

### 2.2.3. The 2 dimensional case

To extend the downstream source term given by relationship (28) to two dimensions we must consider three upstream cells.

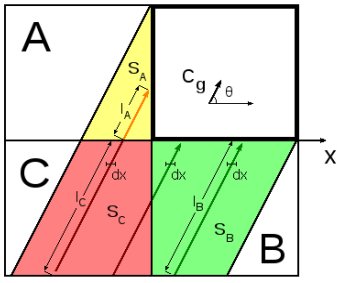


Figure 6: 2-D extension of the downstream source term: the yellow, green and red surfaces $S_A$, $S_B$ and $S_C$ represent the portions of cells A, B and C crossed by the flux towards the examined cell (the upright one). The colored arrows represent flux stripes of infinitesimal width $dx$ crossing the three upstream cells.

Figure 6 illustrates this study case, where the current cell is the up-right one while the upstream cells are A, B and C. Therefore we look for an expression in the form

$$\left.\frac{\partial F}{\partial t}\right|_{d} = -\mathbf{D}\ \{[K_A F_A(F,\alpha_A,\beta_A) + \\ + K_B F_B(F,\alpha_B,\beta_B) + K_C F_C(F,\alpha_C,\beta_C)] - F\} \quad , \tag{34}$$

where $\mathbf{D} = \psi(v)\sqrt{\left(\frac{c_{gx}}{\Delta x}\right)^2 + \left(\frac{c_{gy}}{\Delta y}\right)^2}$ and $K_A$, $K_B$ and $K_C$ are weighting coefficients relative to the upstream cells, such that

$$K_A + K_B + K_C = 1 \quad . \tag{35}$$

A possible approach to estimate $K_A$, $K_B$ and $K_C$ is considering the path length covered across each upstream cell by the energy flux. Referring to figure 6, let us consider the energy within an infinitesimal flux stripe, i.e. a stripe of infinitesimal width $dx$ directed along the flux. In the single stripe the coefficients $K_A$, $K_B$ and $K_C$ can be expressed as

$$\begin{aligned} K_{A\ dx} &= \frac{l_A}{l_A + l_B + l_C} \\ K_{B\ dx} &= \frac{l_B}{l_A + l_B + l_C} \\ K_{C\ dx} &= \frac{l_C}{l_A + l_B + l_C} \quad , \end{aligned} \tag{36}$$

where $l_A$, $l_B$ and $l_C$ are the lengths of the stripes in cells A, B and C respectively. Generally, for any geometry of the problem, lengths $l_A$ and $l_B$ are always different from zero along any flux stripe. Referring to figure 6, for the leftmost stripe only $l_A$ and $l_C$ are not null, while for the other two pictured stripes only $l_B$ and $l_C$ are not null. Using relationships (34) and (36) the formulation for the source term in a single stripe reads:

$$\left.\frac{\partial F}{\partial t}\right|_{d\ dx} = -\mathbf{D}\left[\ \frac{l_A F_A + l_B F_B + l_C F_C}{l_A + l_B + l_C} - F\right] \quad , \tag{37}$$

where the subscript $dx$ stresses the fact that this expression is relative to a single stripe.

Multiplying both members by $(l_A + l_B + l_C)\sin(\theta)dx$ and integrating on the four cells system (on $2\Delta x$) we obtain:

$$\begin{aligned} &(S_A + S_B + S_C)\left\langle \left.\frac{\partial F}{\partial t}\right|_{d\ dx} \right\rangle_{2\Delta x} = \\ &-\mathbf{D}[(S_A F_A + S_B F_B + S_C F_C) - (S_A + S_B + S_C)F] \ , \end{aligned} \tag{38}$$

where $S_A$, $S_B$ and $S_C$ are the surfaces covered by the flux across cells A, B and C (see figure 6) and $\left\langle \left.\frac{\partial F}{\partial t}\right|_{d\ dx} \right\rangle_{2\Delta x}$ is the average value of $\left.\frac{\partial F}{\partial t}\right|_{d\ dx}$ weighted on the relative length of the paths $l_A$, $l_B$ and $l_C$, which is equal to the overall source term. Hence from relationship (38) we obtain the expression of the 2-dimensional source term:

$$\left.\frac{\partial F}{\partial t}\right|_{d} = -\mathbf{D}\left[\ \frac{S_A F_A(F) + S_B F_B(F) + S_C F_C(F)}{S_A + S_B + S_C} - F\right] \quad . \tag{39}$$

The weighting coefficients $K_A$, $K_B$ and $K_C$ introduced in expression (34) are therefore given by

$$\begin{aligned} K_A &= \frac{S_A}{S_A + S_B + S_C} \\ K_B &= \frac{S_B}{S_A + S_B + S_C} \\ K_C &= \frac{S_C}{S_A + S_B + S_C} \quad . \end{aligned} \tag{40}$$

Therefore, using relationship (33) in (39) we obtain the final version of the 2-dimensional shadow source term:

$$\left.\frac{\partial F}{\partial t}\right|_{d} = -\mathbf{D}\left[K_A\left(\frac{\beta_A}{\alpha_A} - 1\right) + K_B\left(\frac{\beta_B}{\alpha_B} - 1\right) + K_C\left(\frac{\beta_C}{\alpha_C} - 1\right)\right]F \quad . \tag{41}$$

### 2.3. The total block problem

A drawback of the approach outlined in the previous sections is that it is unable to handle properly conditions of total block (e.g. unresolved breakwaters extended along a whole cell). In particular if $\alpha$ vanishes SE source term given by expression (33) diverges, and if $\beta$ vanishes LD source term given by expression (19) diverges. Values of $\alpha$ or $\beta$ close to zero would involve very high energy dissipation rates which would dissipate also local energy production. A possible solution is introducing a superior limit to the energy reduction due to the shadow source term, in order to dissipate as much as possible the energy coming from the upstream cell, but not the energy introduced by wind local generation. Therefore for $\alpha$ close to zero LD source term can be expressed as:

$$\frac{\partial F}{\partial t} = -\sqrt{\left(\frac{c_{gx}}{\Delta x}\right)^2 + \left(\frac{c_{gy}}{\Delta y}\right)^2}\,\gamma_{ld} F \,, \tag{42}$$

and SE source term can be expressed as (here we provided only the monodimensional version):

$$\left.\frac{\partial F}{\partial t}\right|_d = -\psi(v)\,\frac{c_g}{\Delta x}\gamma_{se}\,F \quad . \tag{43}$$

For this study we set $\gamma_{ld} = 10$ and $\gamma_{se} = 20$. The reason why the two constants have been set to different values is that when $\beta$ is null, i.e. when expression 42 is used as the LD source term, also $\alpha$ is necessarily null, and formulation 43 is used as the SE source term. Conversely when $\alpha$ is null $\beta$ is not necessarily null, and in such cases an approximate total block must be provided by the sole SE source term. This formulation relies on a proper shape of $\psi(v)$ factor (yet to be provided) in order not to dissipate entirely local energy production in the downstream cell.

## 3. Cases studies: selection and analysis

The source terms outlined in previous section have been validated on a set of nine theoretical case studies using WWIII model. For each case study a synthetic high resolution constant bathymetry (500 $m$ deep) has been generated on a regular grid 80x80 with a resolution of 0.1°, with isolated dry points (or small groups of dry points) representing small islands (see figure 7).

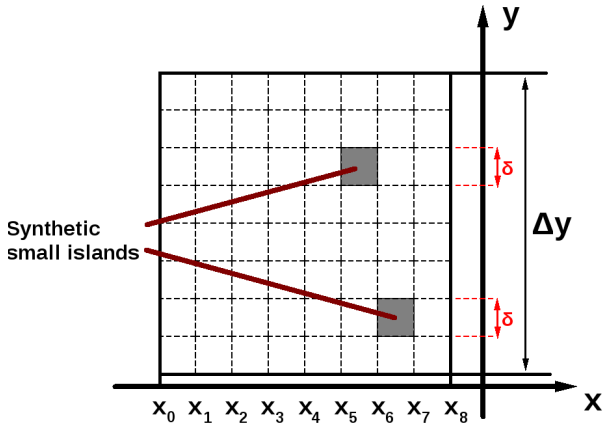


Figure 7: Theoretical case studies: continuous line square represents a low resolution cell, dashed lines represent the corresponding high resolution cells. Gray cells are dry in the high resolution grid, and represent small unresolved islands in the low resolution run.

A corresponding low resolution grid 10x10 has been constructed with a resolution of 0.8°. Side size of low resolution cells is eight times the side size of high resolution ones, so that the effect of "small islands" is resolved in the high resolution run, while in low resolution runs it is parameterized by the source terms or by the standard WWIII approach based on the propagation scheme. For all of the test cases pure swell monodirectional boundary conditions have been imposed, and WWIII model has been employed with no source term active except for LD-SE, in

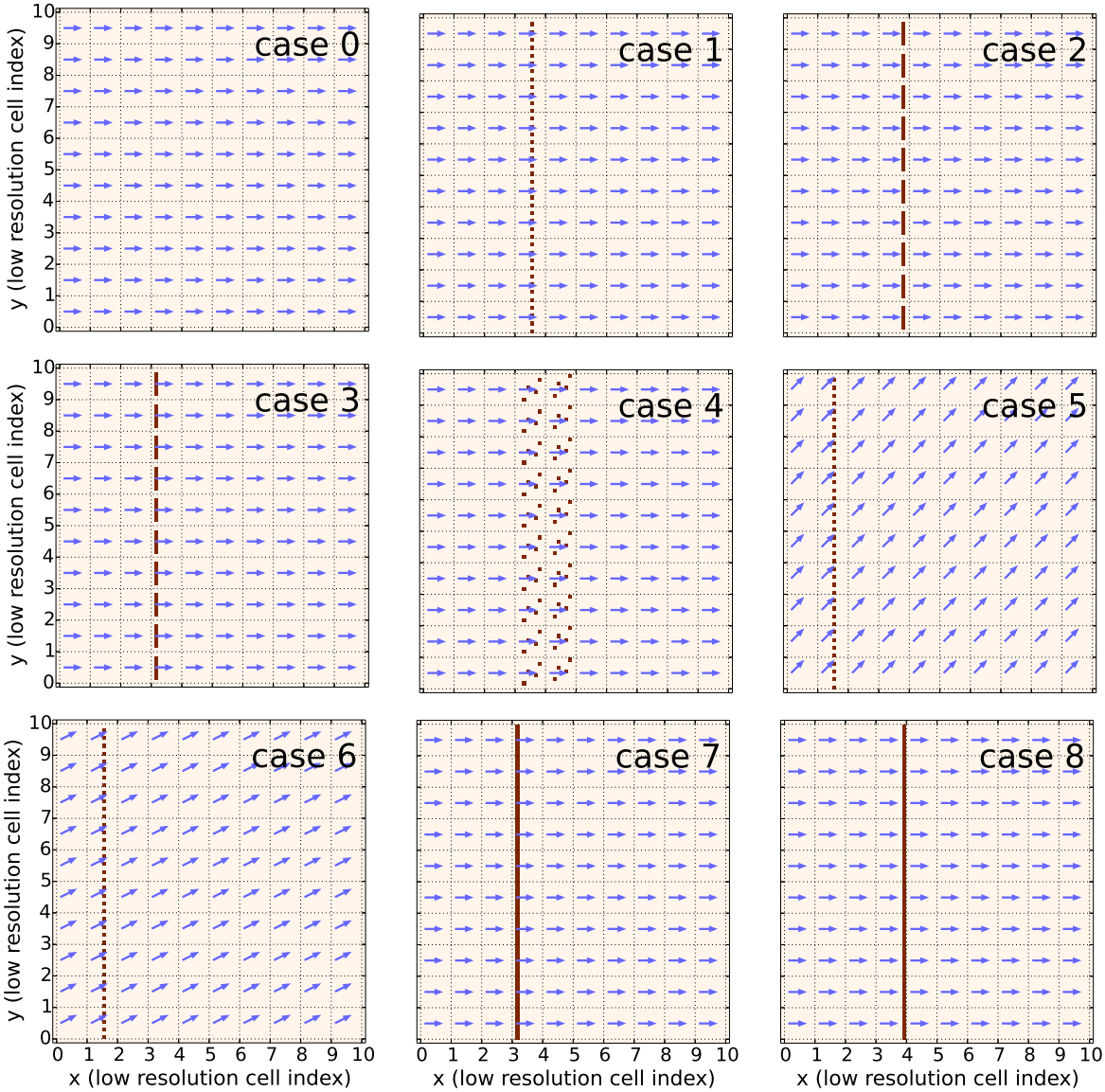


Figure 8: Bathymetry of the elaborated synthetic cases. White cells are 500 $m$ deep, small brown squares are dry cells in the high resolution grid. Blue arrows represent swell direction. Dotted grid is the low resolution one.

order to better isolate and discern the parameterization of unresolved obstacles. For seven of the case studies swell is directed towards the $x$ axis, while in the fifth and sixth case studies it is directed respectively to angles of 45° and 30° clockwise. Hence in correspondence of unresolved islands active generation of waves is absent and the source terms work in pure swell conditions (constant $\psi$ function equal to 1).

For all the case studies the obstacles layout is independent on $y$ direction, guaranteeing uniformity of unresolved obstacles effects in $x$ direction.

Each case study is focused on a different layout of unresolved obstacles or on a different direction of swell, involving a different response of the source terms system (see figure 8). Follows a short description of each case study.

- Case 0: no unresolved obstacles. This case has been modeled to provide an estimation of the intrinsic error due

to a confrontation between high and low resolution models.

- Case 1: unresolved obstacles are located almost in the cell center and are like equally separated islands. Swell is directed towards $x$ axis.
- Case 2: unresolved obstacles are disposed in a continuous block spanning three quarters of the cell crosswise side and close to the downstream side, involving a relatively weak local effect and a strong shadow effect. Swell is directed towards x axis.
- Case 3: unresolved obstacles are disposed in a continuous block as in case 2, but are close to the upstream side, involving a strong local effect and a relatively weak shadow effect. Swell is directed towards $x$ axis.
- Case 4: unresolved obstacles are small islands scattered throughout two consecutive cells. Therefore in the second cell both local and shadow source terms are active. Swell is directed towards x axis.
- Cases 5 and 6: unresolved obstacles layout is like in case 1, but swell is directed respectively to angles of 45° and 30° clockwise, in order to check the source term response to a mainly diagonal energy flux.
- Case 7: total block close to the upstream cell boundary. Swell is directed towards x axis.
- Case 8: total block close to the downstream cell boundary. Swell is directed towards x axis.

### *3.1. Computation of $\alpha$ and $\beta$ coefficients*

For low resolution simulations of the synthetic case studies illustrated above, bidimensional source terms given by expressions (19) and (41) have been employed. Hence a methodology for the estimation of coefficients $\alpha$ and $\beta$ as function of spectral component direction has been developed, on the basis of geometrical considerations on subgrid obstacles layout.

Let us consider a spectral component directed towards the $x$ axis. Coefficient $\alpha$ is computed as the ratio between the size of the obstacles projection to $y$ axis and the size of the $y$ side cell $\Delta y$:

$$\alpha = 1 - \delta_{obs}/\Delta y \,, \tag{44}$$

where $\delta_{obs}$ is the size of the obstacles projection to y-axis. If we consider for example the low resolution cell (figure 7) the value of $\alpha$ is given by $(1 - 2\delta/\Delta y) = 0.75$. The coefficient $\beta$ is estimated as the average of $A_i$ coefficients defined by expression (15). Each $A_i$ is computed using the same considerations drawn for the computation of $\alpha$ coefficient. Referring to figure 7, $A_1$ is estimated as the transparency coefficient of the cell section between $x_0$ and $x_1$, $A_2$ is the transparency coefficient between $x_0$ and $x_2$, $A_N$ between $x_0$ and $x_N$. For the cell represented in figure 7 we have $\beta = \sum(A_i)/8 = (5 + 0.875 + 2 * 0.75)/8 = 0.922$.

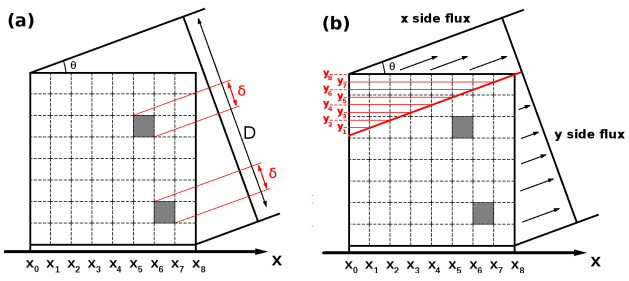


Figure 9: Computation of $\alpha$ (a) and $\beta$ (b) coefficients for a generic spectral component.

Arguments drawn for $x$ direction can be easily extended to the general bidimensional case. Let us consider a spectral component directed to an angle $\theta$ such that $0 < \theta < \pi/4$ from $x$ axis. Coefficient $\alpha$ is given by one minus the ratio of the overall cross section of obstructed cell portion to the cross section of the whole cell. For example in the case illustrated in figure 9 (a) we have $\alpha = 1 - 2\delta/D$.

Computation of $\beta$ coefficient in the case of $0 < \theta < \pi/4$ is illustrated in figure 9 (b). Cell is split into two sections from which energy flows through sides $y$ and $x$ respectively, and the diagonal red line separates the two sections. A transparency coefficient $A_i$ is hence computed for each rectangle having point $x_i$ as its right-bottom vertex, and a point lying on the red line as right-top vertex. Coefficients $A_i$ are estimated employing the same methodology described for $\alpha$ parameter. For example in the cell represented in figure 9 (b), coefficients $A_i$ are computed for rectangles with diagonal points $\{(x_1, y_1), \ ... \ , (x_8, y_8)\}$. An estimation of $\beta$ coefficient is then provided by the average value of $A_i$. A situation of $\theta < 0$ or $\theta > \pi/4$ can be easily connected to the $0 < \theta < \pi/4$ case through appropriate rotations and reflections of $x$ and $y$ axis for both $\alpha$ and $\beta$ coefficients.

## 4. Discussion of results

Simulation results for the synthetic test cases outlined in the previous section are reported in figure 10. Graphs show the average simulated trend of significant wave height along $x$ axis, measured in the central section of the low resolution grid. The different lines in the graphs represent:

- significant wave height simulated for low resolution grid without unresolved obstacles representation (green line).
- Significant wave height simulated for low resolution grid with active $\alpha$-$\beta$ source terms (blue line).
- Significant wave height simulated for low resolution grid using the approach based on the propagation scheme actually implemented in WWIII (Tolman, 2003; Chawla and Tolman, 2008, thin magenta line). Coefficients $\alpha$ employed for these simulations have been estimated following the methodology described in section 3.1.
- Significant wave height simulated for high resolution grid averaged to the low resolution grid cells (continous black line).

In the panels of figure 10 the zones where $\alpha$-$\beta$ source terms act are colored. Light red areas mark cells where the LD source term is active. Light blue areas mark cells where the SE term is active. The violet area indicates cells where the LD-SE source terms are both active.

| *NMAE* | C.0 | C.1 | C.2 | C.3 | C.4 | C.5 | C.6 | C.7 | C.8 |
|---|---|---|---|---|---|---|---|---|---|
| No unr. obs. paramet. | 0.8 % | 28.0 % | 50.6 % | 60.3 % | 54.8 % | 63.8 % | 46.4 % | 271.1 % | 194.8 % |
| Standard approach | 0.8 % | 2.4 % | 2.5 % | 7.0 % | 4.5 % | 24.0 % | 12.0 % | 21.7 % | 4.7 % |
| LD-SE approach | 0.8 % | 1.6 % | 0.9 % | 4.7 % | 1.7 % | 20.4 % | 8.0 % | 14.6 % | 23.4 % |

Table 1: *NMAE* of significant wave height in obstructed low resolution cells for the six case studies, for the model without unresolved obstacles parameterization, the standard WWIII approach and the source term approach.

A comparison between the high spatial resolution simulation representing the obstacles (small islands) and the standard and LD-SE approaches to unresolved obstacles from low resolution simulations is summarized in table 1. The Normalized Mean Absolute Error (*NMAE*) of significant wave hight, defined as

$$NMAE = \frac{\sum |H_i - L_i|}{\sum H_i} \ , \tag{45}$$

where $H_i$ and $L_i$ are the high and low resolution simulated values respectively, is estimated for the nine analyzed case studies. Only cells where wave dynamics are affected by the presence of the unresolved obstacles are considered (cells with $x$ index $i_x \geq 3$ for case studies 1, 2, 3, 4, 7 and 8, and cells with $i_x \geq 1$ for case studies 5 and 6). For all of the analyzed case studies high resolution simulations (which provide the control test of the representation of small islands) are matched rather well by low resolution simulations with the LD-SE scheme. In particular for case studies 1, 2, 3 and 4 *NMAE* of significant wave height between high resolution simulation and low resolution simulation is below 5%. This means that the average representation of unresolved obstacles in those cases is adequate though not error free, since the intrinsic deviation due to resolution reduction is of about 0.8% (see the value of *NMAE* of case 0 in table 1).

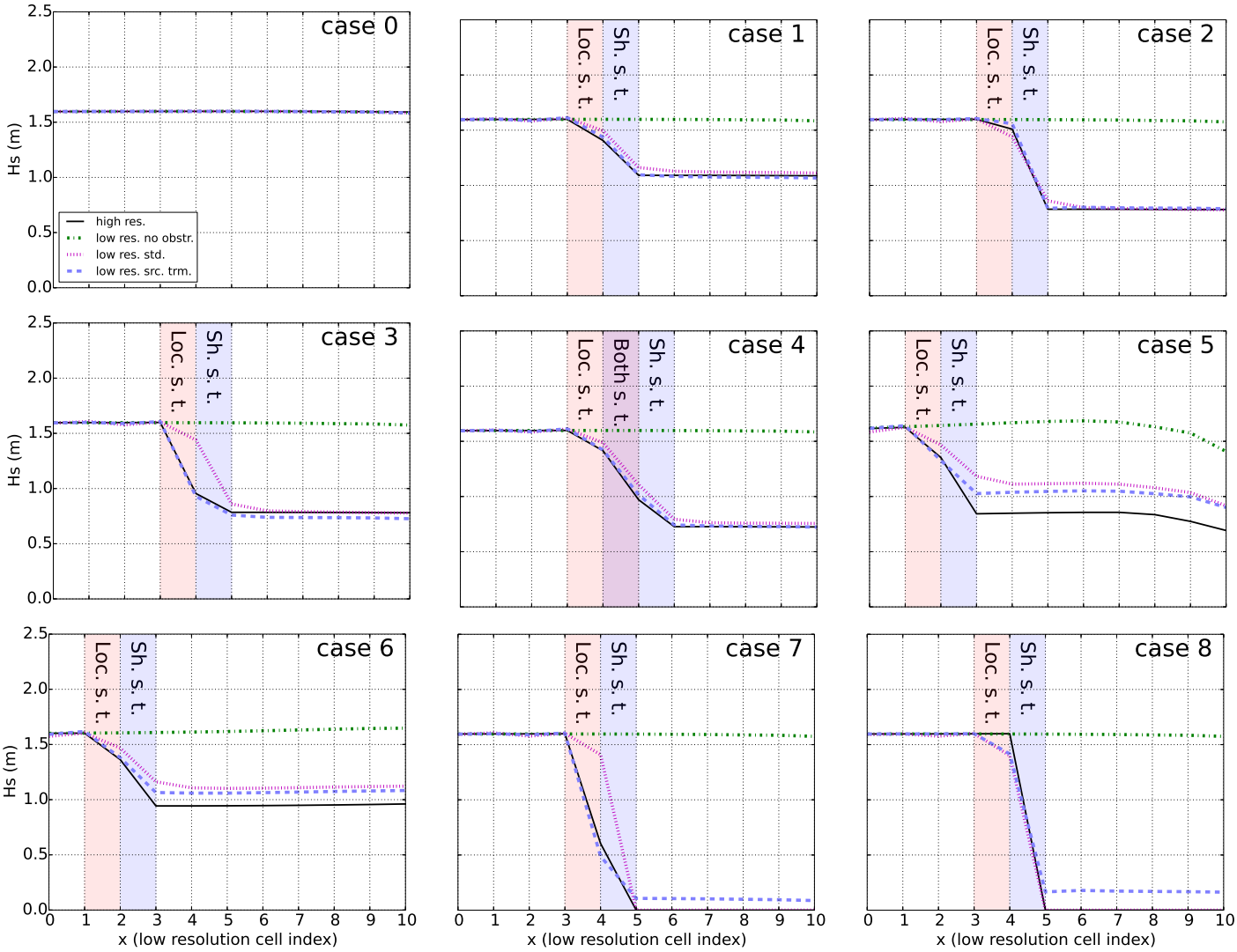


Figure 10: Significant wave height simulated for the elaborated synthetic cases. On x axis is reported the x index of low resolution domain cells. The graphs cover the second half of integration domain. Areas filled with colors evidence cells where the source terms are active.

In case studies 5 and 6 the standard approach and the LD-SE approach present both relatively bad performances. This is due to different reasons for the two approaches. For the standard model the problem is that the small squares that represent unresolved obstacles in cases 5 and 6 present a greater cross section for diagonal modes than for modes directed towards direction x. As a consequence energy dissipation should be greater for diagonal swell than for swell directed towards x axis. However standard WWIII uses transparency coefficients relative to the sole x and y directions. Indeed comparing graphs relative to case 1 and case 5 in figure 10 we can see that for high resolution simulation energy dissipation is greater in case 5 than in case 1, while low resolution simulation with the standard approach models a similar dissipation for the two case studies.

In LD-SE source term we used transparency coefficients modulated with mode direction, therefore the problem with cases 5 and 6 is more related to the methodology employed for the computation of these coefficients. For the evaluation of $\alpha$ and $\beta$ we considered separately each cell. As a result the minimum value of $\alpha$ has been estimated for direction 90°, where $\alpha = 0.5$ (see figure 11, where $\alpha$ coefficient estimated for each direction in obstructed cells of cases 1, 5 and 6 is illustrated). A value of $\alpha = 0.5$ is kept for directions 75°, 60° and 45°, while it increases for

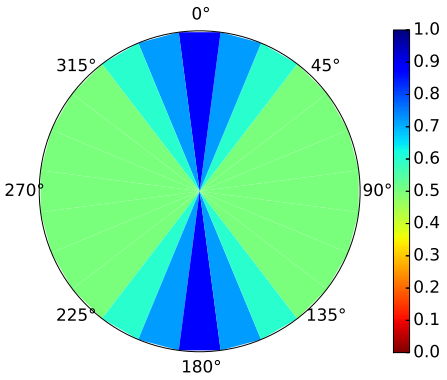


Figure 11: Coefficient $\alpha$ as a function of direction for obstructed cells of case studies 1, 5, and 6.

directions closer to 0°. Those figures are correct if we consider each cell as isolated from the others, indeed local dissipation described by LD source term in obstructed cells is satisfactory, as one can see in figure 10, cases 5 and 6. However the shadow source term is unable to represent properly the combined effect of all the obstructed cells. This effect involves a deeper shadow for energy passing left to right of the line of obstructed cells, due to the above mentioned overall greater cross section of the obstacles for diagonal modes than for modes directed towards direction x. A possible solution to this issue may be using different sets of $\alpha$ and $\beta$ for LD and SE source terms: for LD source term we can continue to consider each cell as isolated from the others, since dissipation is evaluated locally. For SE source term $\alpha$ and $\beta$ should be computed considering the combined effect of the upstream cells.

Cases 7 and 8 represent conditions of total block close respectively to the upstream and the downstream cell side. Parameterization of total block described in paragraph 2.3 (expressions 42 and 43) has been employed. Though the strong dissipation modelled in these cases by LD-SE source term (see figure 10, cases 7 and 8) can be considered as an approximation of a total block, system is unable to eliminate totally the energy leakage left to right of the line of obstructed cells. Better figures could be obtained setting greater values to constants $\gamma_{ld}$ and $\gamma_{se}$, however in general attention should be payed that LD-SE source term should not dissipate the energy produced locally. In this respect a correct formulation of the $\psi(v)$ factor (yet to be provided) is crucial.

For case study 7 the value of *NMAE* estimated for LD-SE source term is lower than that obtained with the standard model. This is due to the better local description of energy dissipation provided by LD-SE source term in cells with $x = 3, x = 4$.

It is finally worth noting that the approximation of total blocking provided by LD-SE source term for case study 7 is better than that provided for case study 8. This is due to the fact that case study 8 has been built in order to have for obstructed cells a value of $\beta$ close to 1 and a vanishing $\alpha$. Therefore in case study 8 the contribution of LD component is weak and most of the dissipation relies on SE source term. Conversely in case study 7 both of LD and SE source terms are contributing to the strong energy dissipation.

## 5. Final remarks

In this work we present a new parameterization of two source terms for unresolved obstacles (the LD-SE scheme). Energy dissipation due to unresolved obstacles is modeled locally, aiming to reproduce in a low resolution grid the average conditions modeled by a high resolution model able to resolve obstacles in an exact way. A shadow source term has been introduced to model the correct energy flux towards downstream cells. This approach potentially allows to overcome some drawbacks of using systems based on energy flux reduction at propagation scheme level, due to a better localization of unresolved obstacles effects. Furthermore this approach treats energy propagation and parameterization of unresolved obstacles as separate things, decoupling those two aspects of wave modelling. A good implementation of the LD-SE scheme would therefore allow not to reformulate, reimplement and revalidate the parameterization of unresolved obstacles for each different propagation scheme. Moreover a source term approach may open the way to parameterizations of unresolved rotation/redistribution over frequencies.

It is worth mentioning that LD-SE scheme impact on the computation costs of WWIII model is small.

The source terms outlined in the present manuscript have been found dependent on two coefficients for each cell and spectral component: a coefficient $\alpha$, representing the overall transparency of the cell, and a coefficient $\beta$ representing the average transparency of cell sections starting from the upstream side. The validation of the source terms has been carried out on nine synthetic case studies, showing their ability to describe the average energy dissipation in a way close to high resolution models able to resolve exactly the obstacles. In many of the case studies the source term approach performs better than the standard approach of WWIII based on the propagation scheme (Tolman, 2003; Chawla and Tolman, 2008). Though LD-SE scheme is in principle unable to handle properly total blocks, as discussed in section 2.3, case studies 7 and 8 show its ability to approximate a correct behavior in such conditions.

A shape of the $\psi(v)$ factor introduced in section 2.2 has not yet been formulated, and this will be a necessary step in order to handle properly local wave generation.

A final remark concerns the computation of $\alpha$ and $\beta$ coefficients. Their estimation is a crucial aspect for the accuracy of any parameterization of unresolved obstacles, and relatively bad performances of both LD-SE scheme and traditional approach in case studies 5 and 6 are due to issues in the computation/employment of these parameters, as explained section 4. Estimation of transparency coefficients is not a trivial task (e.g. Tolman, 2003; Chawla and Tolman, 2008; Hardy et al., 2000), and it is usually accomplished on the basis of geometrical considerations on subscale obstacles layout. In this study we developed a similar methodology to estimate $\alpha$ and $\beta$ for each spectral component, projecting unresolved obstacles to the downstream side of each cell. An alternate approach might be the employment of high resolution stationary wave models initialized with different sets of boundary conditions like monochromatic waves or other elementary wave packages. Such a methodology could provide diagnostic responses of unresolved obstacles throughout the whole spectral space, allowing a more accurate estimation of $\alpha$ and $\beta$ as function not only of spectral component direction, but also of spectral component frequency. Moreover it could allow the definition of additional coefficients useful to parameterize unresolved rotation and redistribution of wave energy over frequencies.

## Acknowledgements

The authors would like to thank Andrea Mazzino of DICCA, University of Genova, who significantly contributed to this project with useful suggestions and insights. This research has been funded by Università degli Studi di Genova through the Progetto di Ricerca di Ateno 2014. We also thank the computational support from the Italian flagship project RITMARE.

## References

Booij, N., Ris, R. C., H., H. L., 1999. A third generation wave model for coastal regions, part i, model description and validation. Journal of Geophysical Research 7 (104), 649–666.

Chawla, A., Tolman, H. L., 2008. Obstruction grids for spectral wave models. Ocean Modelling 22 (22), 12–25.

Hardy, T. A., Mason, B. L., McConochie, J. D., 2000. A wave model for the great barrier reef. Ocean Engineering 28 (28), 45–70.

Hardy, T. A., Young, I. R., 1996. Field study of wave attenuation on an offshore coral reef. Journal of Geophysical Research 14 (101), 311–326.

Holthuijsen, L. H., Booij, N., Ris, R. C., Haagsma, I. G., Kieftenburg, A. T. M. M., Kriezi, E. E., 2001. Swan cycle iii version 40.11 user manual. Tech. rep., Delft University of Technology, Department of Civil Engineering.

Li, J., 2012. Propagation of ocean surface waves on a spherical multiple-cell grid. Journal of Computational Physics 8 (231), 262–277.

Mentaschi, L., Besio, G., Cassola, F., Mazzino, A., 2015. Performance evaluation of wavewatchiii in the mediterranean sea: a 32 years hindcast. Ocean ModellingManuscript submitted for publication.

Ponce de León, S., C., G. S., 2005. On the sheltering effect of islands in ocean wave models. Journal of Geophysical Research 110 (Issue C9).

Roland, A., 2008. Development of wwm ii: Spectral wave modelling on unstructured meshes. Ph.D. thesis, Technische Universitat Darmstadt, Institute of Hydraulic and Water Resources Engineering.

Tolman, H. L., 2001. Improving propagation in ocean wave models. In: Edge, B. L., Hemsley, J. M. (Eds.), 4th international symposium on ocean wave measurement. pp. 70–80.

Tolman, H. L., 2002. Validation of wavewatch iii version 1.15 for a global domain. Technical note 213, NOAA/NWS/NCEP/MMAB.

Tolman, H. L., 2003. Treatment of unresolved islands and ice in wind wave models. Ocean Modelling 5 (5), 219–231.

Tolman, H. L., 2014. User manual and system documentation of wavewatch iii version 4.18. Tech. rep., NOAA/NWS/NCEP/MMAB.

Tuomi, L., Pettersson, H., Fortelius, C., Tikka, K., Bjrkqvist, J., Kahma, K. K., 2014. Wave modelling in archipelagos. Coastal Engineering 83 (83), 205–220.

## Appendix A. Analytical derivation of LD source term

For completeness we rewrite relationship 13 from which the derivation starts.

$$\left.\frac{\partial F}{\partial t}\right|_N = \sum_{i=1}^{N} \phi_i \left.\frac{\partial F}{\partial t}\right|_i \ . \tag{A.1}$$

Applying relationship (4) to each slice we obtain

$$\left.\frac{\partial F}{\partial t}\right|_i = -2\frac{c_g}{\Delta x}\frac{1-\alpha_i}{1+\alpha_i}F_i \ . \tag{A.2}$$

Using A.2 in A.1, and expressing $\phi_i$ as

$$\phi_i = \frac{N-i+1}{N} \tag{A.3}$$

we obtain

$$\left.\frac{\partial F}{\partial t}\right|_N = -2\frac{c_g}{\Delta x}\sum_{i=1}^{N}\frac{N-i+1}{N}\frac{i-\alpha_i}{1+\alpha_i}F_i \ . \tag{A.4}$$

$F_i$ is given by the average energy density of the i-th slice of the cell, which is given by

$$F_i = \frac{\prod_{j=1}^{i-1}\alpha_j F_{u1} + \prod_{j=1}^{i}\alpha_j F_{u1}}{2} = \frac{1+\alpha_i}{2}\prod_{j=1}^{i-1}\alpha_j F_{u1} \ , \tag{A.5}$$

where $F_{u1}$ is the upstream energy density of the first slice, i.e. of the whole cell. Substituting A.5 in A.4

$$\begin{aligned}
\left.\frac{\partial F}{\partial t}\right|_N = & \quad -\frac{c_g}{\Delta x}\sum_{i=1}^{N}\frac{N-i+1}{N}(1-\alpha_i)\prod_{j=1}^{i-1}\alpha_j F_{u1} = \\
= & \quad -\frac{c_g}{\Delta x}\frac{F_{u1}}{N} \\
& \quad \Big[N - N\alpha_1 + (N-1)\alpha_1 - (N-1)\alpha_1\alpha_2 + \\
& \quad + (N-2)\alpha_1\alpha_2 - (N-2)\alpha_1\alpha_2\alpha_3 + ... \\
& \quad + \prod_{j=1}^{i-1}\alpha_j - \prod_{j=1}^{i}\alpha_j\Big] = \\
= & \quad -\frac{c_g}{\Delta x}F_{u1}\Big(1 - \frac{\sum_{i=1}^{N}\prod_{j=1}^{i}\alpha_j}{N}\Big) = \\
= & \quad -\frac{c_g}{\Delta x}F_{u1}(1-\beta) \ .
\end{aligned} \tag{A.6}$$

Now we must express $F_{u1}$ as a function of the average cell energy density $F$. $F$ is given by

$$F = \sum F_i/N \ . \tag{A.7}$$

Using (A.5) in (A.7) one finds

$$\begin{aligned}
F = & \quad \frac{F_{u1}}{2N}\sum_{i=1}^{N}\Big(\prod_{j=1}^{i-1}\alpha_j + \prod_{j=1}^{i}\alpha_j\Big) = \\
= & \quad \frac{F_{u1}}{2N}\Big[1 + 2\Big(\sum\prod_{i=1}^{N-1}\alpha_i\Big) + \prod_{i=1}^{N}\alpha_i\Big] \ .
\end{aligned} \tag{A.8}$$

380 Therefore

$$F_{u1} = \frac{2N}{1 + 2\left[\sum_{i=1}^{N-1} \prod_{j=1}^{i} \alpha_j\right] + \prod_{i=1}^{N} \alpha_i} F \ . \tag{A.9}$$

381 Substituting A.9 in A.6 one obtains

$$\begin{aligned} \left.\frac{\partial F}{\partial t}\right|_N &= -2N \frac{1-\beta}{1 + 2\left(\sum_{i=1}^{N-1} \prod_{j=1}^{i} \alpha_j\right) + \prod_{i=1}^{N} \alpha_i} \frac{c_g}{\Delta x} F = \\ &= -2N \frac{1-\beta}{1 + 2\left(\sum_{i=1}^{N} \prod_{j=1}^{i} \alpha_j\right) - \prod_{i=1}^{N} \alpha_i} \frac{c_g}{\Delta x} F = \\ &= -2N \frac{1-\beta}{1 + 2N\beta - \alpha} \frac{c_g}{\Delta x} F \quad . \end{aligned} \tag{A.10}$$